J. Phys. B: At. Mol. Opt. Phys. **32** (1999) 1269–1294. Printed in the UK PII: S0953-4075(99)97314-5

Adiabatic treatments of vibrational dynamics in low-energy electron–molecule scattering

S Mazevet†§, Michael A Morrison†‖, Olen Boydstun†, and R K Nesbet‡

† Department of Physics and Astronomy, The University of Oklahoma, 440 W Brooks Street, Norman, OK 73019-0225, USA

‡ IBM Almaden Research Center, 650 Harry Road, San Jose, CA 95120-6099, USA

Received 8 September 1998, in final form 8 December 1998

Abstract. Accurate calculations of vibrational excitation cross sections for low-energy electron–molecule collisions require theoretical treatment of dynamical effects due to the vibrational kinetic energy operator. As alternatives to solving the integrodifferential equations that describe coupled electronic and vibrational motion, adiabatic methods, which parametrize the internuclear geometry, offer practical and conceptual simplifications. Here we investigate two such methods: the energy-modified adiabatic phase matrix method, which retains the vibrational kinetic energy in the fixed-nuclei scattering matrix and approximates the continuum energy, and the first-order non-degenerate adiabatic approximation, which evaluates fixed-nuclei scattering matrices off the energy–momentum shell in order to ensure strict conservation of energy. The present implementation of these methods is improved over previous versions. They are assessed against benchmark results from converged vibrational close-coupling calculations. Specifically, we compare integral and differential $0 \rightarrow 1$ and $0 \rightarrow 2$ cross sections for e–H_2 scattering at energies from their respective thresholds to 10 eV.

1. Introduction

The central conundrum in the theoretical study of low-energy inelastic vibrational excitation of molecules by electron impact is how to incorporate the effect of the nuclear kinetic energy operator on the wavefunction of the scattering electron. The implications of this issue range beyond vibrational excitation to the generic problem of a quantum mechanical phenomenon that depends on a more-or-less slowly varying coordinate. For low-lying vibrational excitations, the periods typical of the initial and final target states (on the order of 10^{-14} s) are much less than typical collision times, so the internuclear separation (R for a diatomic target) can be treated adiabatically. Since the earliest investigations of vibrational excitation that were based on theories more sophisticated than weak-scattering approximations, two approaches to this conundrum have predominated. (For work prior to 1980, see Lane (1980).) On the one hand, the effects of the vibrational Hamiltonian can be taken into account rigorously (in principle, at least) by expanding the electron–molecule wavefunction in a complete set of eigenfunctions of this Hamiltonian—as in, for example, laboratory-frame (Henry 1970, Morrison *et al* 1984a, b) and body-frame (Chandra and Temkin 1976, Morrison and Trail 1993, Morrison and Sun 1995) vibrational close-coupling (VCC) calculations. On the other hand, these effects can

§ E-mail address: MAZEVET@MAIL.NHN.OU.EDU

‖ E-mail address: MORRISON@MAIL.NHN.OU.EDU

0953-4075/99/051269+26$19.50 © 1999 IOP Publishing Ltd

be approximated by treating the internuclear separation of the molecule as a parameter—in effect, extending the conventional Born–Oppenheimer theory of bound molecular states to the continuum states of the electron–molecule system (Chase 1956, Shugard and Hazi 1975). This approach is the foundation of the conventional adiabatic nuclear vibration (ANV) approximation (Faisal and Temkin 1972). For scattering near the energy of a reasonably long-lived resonance, the *R*-matrix (Schneider *et al* 1979a), projection operator (Domcke 1991), and nonadiabatic phase matrix (NADP) (Mazevet *et al* 1998, 1999) methods offer physically appropriate alternatives.

The numerical and computational difficulties attendant upon VCC calculations render them applicable only to the very simplest electron–molecule systems (see Morrison and Sun (1995) and references therein). While ANV calculations are not without their difficulties, they can be performed on a far greater range of systems (for reviews, see Lane (1980) and Morrison (1988) and references therein). Since the mid-1980s, however, the ANV approximation has been known to introduce significant error into vibrational cross sections for scattering energies near and within a few eV above an excitation threshold (Morrison *et al* 1984a, b). The primary source of this error (for non-resonant scattering) is the assumption, inherent in the ANV method, that the energy lost by the electron due to excitation of the target is negligible compared to the incident kinetic energy. Thus ANV calculations do not conserve total energy through the collision. During the last decade, several schemes have been proposed which preserve the highly desirable adiabatic separation of the nuclear motion from that of the scattering electron without incurring the error attendant upon ANV calculations (for a review, see Morrison (1988)).

These alternative adiabatic approximations fall into two categories, depending on whether or not they use fixed-nuclei transition (T) matrices calculated off the energy–momentum shell (see the survey in section V of Morrison (1988)). Off-shell methods, such as the first-order non-degenerate adiabatic (FONDA) approximation (Morrison 1986, Abdolsalami and Morrison 1987, Morrison *et al* 1991), ensure conservation of energy by explicitly evaluating fixed-nuclei scattering matrices at precisely the point in the complex momentum plane that corresponds to the correct entrance- and exit-channel energies. The other class of methods, such as the energy-modified approximation (EMA), retain the nuclear kinetic energy operator explicitly in the fixed-nuclei scattering matrix, which itself becomes an operator, then introduce approximations to the continuum energy in order to transform the resulting operator functions into functions of energy (Nesbet 1979, Thümmel *et al* 1992). Both classes of methods require more computational power than a conventional ANV calculation but far less than a converged VCC calculation.

This paper explores one of each of these alternative types of adiabatic approximations—the FONDA and EMA methods—in the context of a system for which highly reliable ANV and VCC cross sections are available: electron scattering from molecular hydrogen. We here extend our earlier work on the $0 \rightarrow 1$ excitation in this system (Morrison *et al* 1984b, 1991) to the $0 \rightarrow 2$ transition. Because the insight that inelastic integral cross sections provide into the central questions of this research are limited, we also compare differential cross sections.

In order to ensure that the differences between cross sections from various calculations actually reflect their different treatments of the nuclear dynamics, we have used a consistent representation of the electron–molecule interaction potential and the vibrational wavefunctions, and imposed a consistent (high) level of numerical precision. We use an interaction potential which includes electrostatic and exchange interactions exactly (within a Hartree–Fock representation of the electronic target state) and correlation-polarization effects exactly except within the target-electron density; this potential has been shown accurate for low-lying excitations in earlier publications from this group (Morrison *et al* 1987, Crompton and

Morrison 1993). The vibrational wavefunctions are based on numerical solution of the nuclear Schrödinger equation, as described in section II.C of Trail *et al* (1990).

Section 2 of this paper summarizes the VCC, ANV, FONDA, and EMA approaches, while section 3 discusses their implementation. In section 4 we compare integral and differential cross sections from various methods, giving particular attention to near-threshold energies, a regime that highlights the practical consequences of theoretical differences between these methods.

2. Theoretical background

Detailed accounts of the VCC, FONDA, and ANV calculations can be found in the indicated references in section 1. Here we summarize points about these methods required for the procedural and implementation details of section 3 and note features of the EMA phase-matrix (EMAP) method that will pertain to the results in section 4.

2.1. The body-frame fixed-nuclear orientation description of the collision

The essential approximations underlying this study are (1) reduction of the electron–molecule Schrödinger equation to an equation for scattering from the molecule in the (Born–Oppenheimer) ground electronic state, and (2) neglect of the rotational kinetic energy in the resulting system Hamiltonian for justifications and references, see Lane (1980), Morrison (1988), Morrison and Sun (1995). The first approximation is appropriate for scattering energies where electronic excitation is energetically forbidden or highly unlikely, provided one incorporates bound-free correlation and polarization effects in the interaction potential—e.g., via an optical potential (see, for example, Meyer *et al* (1992) and Collins and Schneider (1981)) or, as here, via a local model potential.

The second approximation, the fixed-nuclear-orientation (FNO) approximation, in effect eliminates the rotational degrees of freedom from the scattering problem (Chase 1956, Temkin and Vasavada 1967, Hara 1969, Chang and Fano 1982). This approximation is an appropriate (and convenient) way to deal with the rotational dynamics in a study of *vibrational* excitation, for which threshold energies are typically an order of magnitude or more larger than for rotational excitations, and measurements on most system cannot resolve initial or final rotational states.

Within the FNO approximation, the most convenient reference frame is the body frame (BF) which, for electron scattering from a linear molecule, is one whose z axis is coincident with the internuclear orientation $\hat{\boldsymbol{R}}$. In this frame, the (reduced) system wavefunction $\Psi_{E,v_0}(\boldsymbol{r}, R)$ depends on four spatial coordinates: one for internuclear separation R and three for the continuum electron, $\boldsymbol{r}$. The quantum number v_0 signifies the initial vibrational state of the target, and the total system energy E is related to the initial and final vibrational energies E_0 and E_v by energy conservation, as

$$E = \tfrac{1}{2}k_0^2 + E_0 = \tfrac{1}{2}k_v^2 + E_v, \tag{1}$$

where $k_0^2/2$ and $k_v^2/2$ are the kinetic energies of the projectile in the entrance and exit channels in hartree†. As the zero of energy we choose the energy of the ground vibrational state E_0. Therefore the threshold energy $\Delta\epsilon_v$, the energy lost by an electron that induces a transition $v_0 \rightarrow v$, is

$$\Delta\epsilon_v = E_v. \tag{2}$$

† Unless otherwise noted, we use hartree atomic units throughout this paper.

To further reduce the Schrödinger equation to a set of coupled radial integrodifferential equations, we expand $\Psi_{E,v_0}(\boldsymbol{r}, R)$ in a basis suitable to the BF FNO formulation. In this approximation the projection Λ of the total electronic orbital angular momentum on the internuclear axis is a constant of the motion. (For closed-shell targets, this angular momentum equals that of the projectile.) So a convenient basis is $\{|v, \ell; \Lambda\rangle\}$, where ℓ is the orbital angular momentum quantum number of the projectile and the semicolon denotes the special status of its projection Λ. The resulting radial equations are coupled in v and ℓ but not in Λ. In configuration space, this basis is $\{\chi_v(R)Y_{\ell\Lambda}(\hat{r})\}$, where $\chi_v(R)$ is a target vibrational function. For homonuclear targets, the parity η is also a constant of the motion, so the vibronic T-matrix for incident energy $E_0 = k_0^2/2$ with initial and final channels $|v_0\ell_0; \Lambda\rangle$ and $|v\ell; \Lambda\rangle$ is $T_{v\ell,v_0,\ell_0}(E_0)$. We suppress the projection quantum number Λ and the parity, it being understood that all fixed-nuclei quantities are referred to a particular values of these quantities.

2.2. Approximations to vibrational effects

At issue in the present research is the effect of molecular vibrations on the scattering function. Expansion of $\Psi_{E,v_0}(\boldsymbol{r}, R)$ in the FNO basis $\{|v, \ell; \Lambda\rangle\}$ leads to radial equations in which these effects are incorporated rigorously through the coupling amongst the radial scattering functions $u_{v\ell,v_0\ell_0}(r)$ by the R-dependent interaction potential. Moreover, in these VCC equations, the energy of the projectile after excitation is $k_v^2/2$, in accordance with the energy conservation equation (1).

But the set of VCC equations contains an infinite number of equations, and, even neglecting those due to the vibrational continuum (dissociation channels), that is too many to solve. Only for H_2 have these equations been solved to convergence in a formulation that treats non-local exchange effects exactly and neglects the vibrational continuum (Trail *et al* 1990, Trail 1991), and only recently have they been solved for N_2 (Weatherford and Temkin 1994, Sun *et al* 1995).

As alternatives to the VCC method we here consider three approximate formulations: the conventional ANV method, the FONDA method, and the EMA approximation. Although formally quite different, these methods share a common approach to the effects of vibration on scattering quantities: all treat the internuclear coordinate R adiabatically. This stratagem amounts to imposing a Born–Oppenheimer separation *on the continuum electron–molecule wavefunction* (Shugard and Hazi 1975). This approach amounts to replacing the FNO expansion basis $\{|v, \ell; \Lambda\rangle\}$ by $\{|\ell; \Lambda\rangle\}$ and eliminating vibrations from the scattering problem altogether. Structurally, these adiabatic methods approximate the FNO scattering matrix $T_{v\ell,v_0,\ell_0}$ by an integral over R in matrix elements of the form

$$T_{v\ell,v_0,\ell_0} \approx \langle\chi_v|T_{\ell,\ell_0}(R)|\chi_{v_0}\rangle. \tag{3}$$

Physically these methods differ in their treatment of the energetics of the collision. In practice they are variously formulated in terms of the scattering (S), reactance (K), or transition (T) matrices, as discussed in the following sections.

2.2.1. The adiabatic nuclear vibration method. If one imposes the continuum Born–Oppenheimer approximation on $\Psi_{E,v_0}(\boldsymbol{r}, R)$ and does nothing more, one obtains the ANV method. For a given electron–molecule symmetry, one merely solves the BF scattering equations,

$$[\hat{T}_e(R) + V_{\mathrm{SEP}}(\boldsymbol{r}; R) - \epsilon]w_{\ell,\ell_0}(r; R) = 0, \tag{4}$$

where $V_{\mathrm{SEP}}(\boldsymbol{r}; R)$ is an appropriate fixed-nuclei static-exchange-polarization potential and ϵ is the continuum (body) energy ϵ. One then extracts the T-matrix from the resulting adiabatic

scattering functions $w_{\ell,\ell_0}(r;\,R)$ in the asymptotic region and calculates an approximate vibronic T-matrix from equation (3). For scattering energies E_0 near an excitation threshold $\Delta\epsilon_v$, this method loses accuracy because it violates the conservation of energy equation (1). The resulting error in ANV cross sections grows dramatically as the incident energy decreases to threshold.

Two features of ANV approximations are germane to the other methods considered here. First, parametrization of R in the continuum Born–Oppenheimer approximation divorces the resulting fixed-nuclei scattering equations from information about the energy lost by the electron when it induces a transition $v_0 \rightarrow v$. That is, the ANV approximation renders indeterminate the energy ϵ in equations (4). This freedom liberates one to choose any body energy one likes: various ANV implementations have set this 'body energy' equal to the incident kinetic energy E_0 (Chase 1956), the final kinetic energy E_v (Chang and Temkin 1970), or some value between the two (Nesbet 1979, Thümmel *et al* 1992). Second, as the scattering energy decreases towards threshold, the ANV vibronic T-matrix elements violate the threshold laws required by quantum mechanics (Morrison *et al* 1984a, Morrison 1988, Thümmel *et al* 1995),

$$T_{v\ell,v_0,\ell_0} \underset{k_v\rightarrow 0}{\longrightarrow} k_v^{\ell+1/2}, \tag{5}$$

where k_v is the wavenumber of the electron in the exit channel. To partially correct the second defect, most implementations multiply the ANV inelastic T-matrix by a 'flux factor', the ratio k_v/k_0. Although this gambit has no theoretical foundation *per se* and does not restore the proper threshold laws, it does ensure that all inelastic ANV T-matrix elements—and hence ANV cross sections—go to zero at threshold.

2.2.2. The first-order non-degenerate adiabatic approximation. The second approximation under consideration, the FONDA method, implements the continuum Born–Oppenheimer strategy by approximating the system wavefunction in a particular symmetry by the product of an *adiabatic scattering function* $w_{\ell,\ell_0}(r;\,R)$ for the projectile and the *ground-state* vibrational function $\chi_{v_0}(R)$, as

$$\Psi_{E,v_0,\ell_0}(\boldsymbol{r},\,R) \approx w_{\ell,\ell_0}(r;\,R)\chi_{v_0}(R), \tag{6}$$

where ℓ_0 denotes the orbital angular momentum of the projectile in the entrance channel. The resulting theory, although strictly adiabatic, restores energy conservation (1) within the vibrationally adiabatic framework of equation (3) by evaluating the fixed-nuclei scattering matrix $T_{\ell,\ell_0}(R)$ off the energy–momentum shell (Chase 1956, Shugard and Hazi 1975). While in the ANV method, this matrix is evaluated on-shell at the arbitrary body energy ϵ, in the FONDA formalism it is evaluated (via the post form of the integral equation for the fixed-nuclei T-matrix) at the proper entrance- and exit-channel wavenumbers k_0 and k_v. In addition to guaranteeing energy conservation, the FONDA approach, by requiring the ground-state vibrational function in equation (6), unambiguously specifies the channel energies. Most importantly, this is the only of the three adiabatic methods under consideration in which all elements of the vibronic T-matrix rigorously satisfy the required threshold laws equation (5). These improvements greatly increase the accuracy of FONDA cross sections, especially near threshold (Abdolsalami and Morrison 1987). To everything there is a price, however: the FONDA method requires an additional integration (over r) for each transition and incident energy. Furthermore, the FONDA method is not strictly unitary, so if unitarity is important, one must restore this property, as discussed in section 3.

2.2.3. The energy-modified adiabatic approximation. The EMA approximation takes a completely different tack. Nesbet's (1979) initial presentation of this method showed that

the exact vibronic S-matrix is formally equal to an integral over R of the form (3) *in which the body energy ϵ in the fixed-nuclei S-matrix is replaced by an energy-shifted vibrational kinetic energy operator*, as

$$S_{v,v_0} = \langle \chi_v | \hat{S}(E - \hat{T}_v - \mathcal{E}^{(e)}; R) | \chi_{v_0} \rangle. \tag{7}$$

Here $\hat{T}_v$ is the vibrational kinetic energy operator, E is the total energy (1), $\hat{S}$ is the fixed-nuclei scattering operator, and $\mathcal{E}^{(e)}(R)$ is the (Born–Oppenheimer) electronic energy of the ground state of the target. This replacement not only restores energy conservation but also incorporates rigorously the dynamical interplay between the continuum electron and vibrations of the target molecule. It is therefore valid under circumstances that cause other adiabatic approximations to fail—e.g., near a shape resonance with an intermediate or long lifetime.

The price for this boon is that in practice one must invoke approximations to render the formal result (7) calculable. Thus Nesbet (1979) suggested approximating the fixed-nuclei EMA S-matrix elements by

$$S_{v\ell,v_0,\ell_0} \approx \langle \chi_v | S_{\ell,\ell_0}(\epsilon; R) | \chi_{v_0} \rangle, \tag{8}$$

where the (vibrationally) diagonal elements are evaluated at $E - E_v$ and the off-diagonal elements at the geometric mean $\epsilon = \epsilon_{v,v_0}$ of E_0 and E_v,

$$\epsilon_{v,v_0} = \sqrt{(E - E_v)(E - E_0)}. \tag{9}$$

Using the geometric mean for the body energy ensures that the resulting approximate EMA T-matrix elements will obey the threshold law (5). The approximation of replacing $\hat{\epsilon}$ by the geometric mean is appropriate to the threshold law for short-range interactions. It loses validity, however, for long-range potentials and under conditions where vibronic interactions are strong. To ensure unitarity of the EMA vibronic T-matrix, Nesbet recommended implementing the analogue of equation (8) *for the K-matrix*. Being symmetric, this K-matrix necessarily produces a unitary vibronic T-matrix.

3. Implementation

In this section we note salient features of the practical implementation of the methods introduced in section 2.

3.1. The adiabatic nuclear vibration method

The key equation of the ANV method is equation (3) for the BF fixed-nuclei T-matrix. In this paper, we determine this matrix from the asymptotic behaviour of the solution of the integrodifferential scattering equations (4), choosing the body energy to be the *incident* kinetic energy of the projectile, $\epsilon = E_0$. In practice, we apply (real) K-matrix boundary conditions

$$w_{\ell,\ell_0}(r; R) \underset{r\to\infty}{\longrightarrow} \hat{j}_\ell(k_0 r)\delta_{\ell,\ell_0} + K_{\ell,\ell_0}\hat{n}_\ell(k_0 r), \tag{10}$$

where $\hat{j}_\ell(k_0 r)$ and $\hat{n}_\ell(k_0 r)$ are the Ricatti–Bessel and Ricatti–Neumann functions in the conventions of (Taylor 1972). The T-matrix corresponding to this K-matrix is

$$\mathsf{T} = \mathsf{K}(\mathsf{1} - \mathrm{i}\mathsf{K})^{-1} \tag{11}$$

for the convention adopted here, that $\mathsf{S} = \mathsf{1} + 2\mathrm{i}\mathsf{T}$ (see the appendix to Morrison and Sun (1995) for transformation equations appropriate to alternative conventions).

As noted in section 2, the resulting ANV differential cross sections and corresponding integral cross sections do not go to zero at threshold $k_v \to 0$. Following standard practice, we *enforce* this behaviour by multiplying these cross sections by the flux factor k_v/k_0; we shall refer to these *corrected* ANV cross sections by the acronym ANVf.

3.2. The phase matrix

Our implementation of the EMA method uses Nesbet's (1979) recommended approximation to the EMA reactance matrix, the K-matrix analogue of equation (7). Because this approach requires construction of the vibronic T-matrix for the transition $v_0 \rightarrow v$ from an EMA vibronic K-matrix, several practical points of implementation require careful attention.

(i) The conversion (11) of the vibronic K-matrix to the vibronic T-matrix shuffles elements of K with different vibrational indices. If we consider a block structure of the K-matrix which groups together elements $K_{v''\ell'',v'\ell'}$ with the same vibrational quantum numbers (v'', v'), then one must converge the T-matrix elements corresponding to the desired transition, $v_0 \rightarrow v$, with respect to blocks of the K-matrix. In e–H_2 scattering, this problem arises only for the Σ_u symmetry. That is, one cannot calculate accurate Σ_u T-matrix elements for this transition from vibrational blocks (v, v_0) alone; rather, one must include in the conversion (11) blocks $\mathsf{K}^{\Lambda}_{v'',v'}$ for additional pairs of quantum numbers (v'', v'). This property is illustrated for the $0 \rightarrow 1$ transition in table 1. This problem also arises in conversion between the phase matrix and the K-matrix.

Table 1. Partial e–H_2 $0 \rightarrow 1$ vibrational excitation cross sections in the Σ_u symmetry from calculations using the ANVf and EMAP methods. Three EMAP calculations are represented: the cross sections labelled EMAP1 were determined by using only one vibrational (v'', v') submatrix of the EMAP K-matrix, the submatrix corresponding to $v'' = 0$ and $v' = 1$, in the conversion of this K-matrix to the T-matrix for the $0 \rightarrow 1$ excitation. The EMAP2 and EMAP3 results were determined with vibrational submatrices of the EMAP K-matrix corresponding to additional vibrational functions: EMAP2 includes states with vibrational quantum numbers 0, 1, and 2, and EMAP3 includes these three states and $v' = 3$.

Energy (eV)	ANVf	EMAP1	EMAP2	EMAP3
0.52	0.2945	0.2945	0.2929	0.2924
0.54	0.3130	0.3136	0.3117	0.3111
0.56	0.3313	0.3325	0.3303	0.3296
0.58	0.3509	0.3528	0.3502	0.3493
0.60	0.3705	0.3733	0.3702	0.3692
0.65	0.4215	0.4268	0.4224	0.4209
0.70	0.4751	0.4836	0.4774	0.4753
0.75	0.5308	0.5433	0.5347	0.5319
0.80	0.5883	0.6054	0.5940	0.5902
0.85	0.6477	0.6701	0.6550	0.6502
0.90	0.7082	0.7364	0.7171	0.7112
0.95	0.7705	0.8051	0.7807	0.7737
1.00	0.8324	0.8739	0.8437	0.8355
1.20	1.0826	1.1570	1.095	1.0830
1.40	1.3173	1.4290	1.327	1.1314
1.60	1.5191	1.6690	1.522	1.5130
1.80	1.6803	1.8670	1.676	1.6730
2.00	1.7967	2.0120	1.786	1.7910
3.00	1.8637	2.1170	1.844	1.8640
4.00	1.5456	1.7410	1.537	1.5460
5.00	1.2016	1.3360	1.20	1.2020
6.00	0.9254	1.0160	0.9276	0.9256
7.00	0.7191	0.7811	0.7223	0.7193
8.00	0.5678	0.6110	0.5710	0.5680
9.00	0.4563	0.4871	0.4591	0.4565
10.00	0.3719	0.3944	0.3743	0.3721

(ii) Each vibrational block $\mathsf{K}^{\Lambda}_{v'',v'}$ must be evaluated for body energy ϵ equal to the energy specified by the EMA prescription: diagonal blocks at $E_{v'} = E_{v''}$, off-diagonal blocks at the geometric mean (9). Because of point (i) above, in practice a large number of these blocks must be evaluated. While one could generate all these blocks by solving the fixed-nuclei scattering equation (4) repeatedly, we prefer to interpolate elements determined on a fixed energy grid of body energies ϵ.

(iii) The fixed-nuclei K-matrix $\mathsf{K}(E_0; R)$ is ill-behaved as a function of E and R because it manifests a regular series of asymptotes. These afflict the numerical quadratures required to evaluate vibrational integrals over this matrix. They also cause problems in numerical interpolation of the aforementioned fixed-nuclei K-matrix elements with energy.

The key to coping with these technical difficulties is the phase matrix. In the present implementation, we define the phase matrix as the inverse tangent of the fixed-nuclei K-matrix,

$$\mathbf{\Phi}(\epsilon; R) \equiv \tan^{-1} \mathsf{K}(\epsilon; R). \tag{12}$$

This device is related to the familiar eigenphase sum $\delta_{\rm sum}$, which is conventionally constructed by diagonalizing $\mathbf{\Phi}$ and summing the resulting eigenphases δ_i (the trace of the phase matrix, an invariant, is the eigenphase sum). The tremendous advantage of the phase matrix is that its elements are free of singularities. Moreover, it greatly facilitates interpolations with respect to energy and internuclear separation. The use of the phase matrix in an EMA calculation was first suggested by Nesbet (1991); this matrix assumes a vital role in the NADP method. As its name implies, the latter method incorporates nonadiabatic effects (in an approach based on fixed-nuclei R-matrices) for scattering conditions where such effects are important, such as near-resonant collisions. (For details, see Nesbet (1996), Thümmel *et al* (1995), Mazevet *et al* (1999).)

From the phase matrix one can determine the eigenphase sum and then construct the fixed-nuclei partial integral cross sections for homonuclear targets as

$$\sigma^{\Lambda_\eta}(E_0; R) = \frac{4\pi}{k_0^2} \sum_{\Lambda=0}^{\infty} (2 - \delta_{\Lambda,0}) \sin^2 \delta_{\rm sum}. \tag{13}$$

The sum of these results is the fixed-nuclei approximation to the vibrationally elastic cross section, the sum over all rotational states of all rotational transitions within the vibrational manifold of interest (Lane 1980). (The prefactor $(2-\delta_{\Lambda,0})$ accounts for the twofold degeneracy of all electron–molecule symmetries except Σ_g.) Thus the starting point for the generation of the EMAP vibronic K-matrix is a set of fixed-nuclei phase matrices on a grid of internuclear separations and evenly spaced body energies.

Later in this section we present graphs of eigenphase sums as functions of body energy and/or internuclear separation. These results are obtained by diagonalizing the phase matrices, to obtain eigenphase shifts $\delta_i(R)$, i.e.,

$$\delta_i(R) = \sum_{\ell'} \langle i|\ell'; \Lambda\rangle \mathbf{\Phi} \langle \ell'; \Lambda|i\rangle, \tag{14}$$

where the index i runs from 1 to the number of eigenphases. We have added multiples of π to the eigenphases in order to ensure smooth variation in both body energy ϵ and internuclear separation R.

3.3. The energy-modified adiabatic phase matrix method

Construction of the EMAP proceeds in four steps. The first two are repeated for each vibrational block (v'', v') of the vibronic K-matrix required to converge the desired block (v, v_0) of the vibronic T-matrix (see table 1).

(i) Interpolate elements of the fixed-nuclei phase matrix with respect to energy to obtain elements at the geometric mean energy $\epsilon_{v'',v'}$.

(ii) Construct matrix elements of the vibronic phase matrix by quadrature over R, interpolating as required by

$$\mathbf{\Phi}_{v'',v'}(E) \approx \langle \chi_{v''} | \mathbf{\Phi}(\epsilon_{v'',v'}; R) | \chi_{v_0} \rangle. \tag{15}$$

(iii) Construct the vibronic K-matrix from the full vibronic phase matrix.

(iv) Transform this vibronic K-matrix to a T-matrix via equation (11) and select from it the vibrational block (v, v_0) for the desired $v_0 \rightarrow v$ transition. To ensure convergence of the former, we include partial waves of order higher than those included in the solution of the fixed-nuclei scattering equations (4) via numerical and analytic completion of the sums over partial wave order (Isaacs and Morrison 1998). Thus, in solving the scattering equations we use three partial waves per symmetry, but in evaluating cross sections we include 10 per symmetry.

Figures 1–3 show two perspectives on the fixed-nuclei eigenphase sums. Figures 1 and 2 focus on the variation of these quantities with body energy ϵ for fixed internuclear separations. The Σ_g and Π_u eigenphase sums in figure 1 illustrate the smooth variations with R that typify non-resonant electron–molecule systems (for other examples, see Lane (1980) and Morrison (1988)). The Π_g symmetry makes negligible contributions to e–H_2 cross sections at these energies and hence are not shown.

In contrast, the Σ_u eigenphase sums in figure 2 show that with increasing internuclear separation, the variation of this quantity with energy becomes much more rapid. For $R > 1.8\ a_0$, the eigenphase sums manifest a fixed-nuclei shape resonance whose width decreases as the internuclear separation increases further (this resonance has been exhaustively studied; see, for example, Nesbet *et al* (1984) and references in Lane (1980)). Increasing the internuclear separation strengthens the (fixed-nuclei) interaction potential, drawing the resonance pole closer to the real energy axis until, by $R \approx 2.8\ a_0$, the Σ_u state becomes bound (McCurdy and Mowrey 1982, DeRose *et al* 1985, Gorczyca and Norcross 1990). The curve for $R = 2.5\ a_0$ shows that this resonance is associated with a background eigenphase sum which decreases with energy. Note, however, that this resonance is not well defined in the vicinity of the equilibrium separation, $R = 1.4\ a_0$, where the peak in the ground vibrational wavefunction occurs. Indeed, for $R \leqslant 1.8\ a_0$, the Σ_u eigenphase sum does not even pass through $\pi/2$; as such, its status as a resonance is dubious (Hazi 1979). At still smaller internuclear separations it becomes indistinguishable from the background. Because of the extremely short lifetime of this resonance, adiabatic methods like the ANV, EMA, and FONDA yield quite accurate $0 \rightarrow 1$ cross sections, even though resonance scattering is usually sensitive to nonadiabatic effects these approximations neglect (see section 4). Additional consequences for vibrational excitation calculations of the ambiguous character of this resonance are addressed in Mazevet *et al* (1998, 1999).

Figure 3 complements figures 1 and 2 by showing the variation with internuclear separation of the Σ_u and Π_u eigenphase sums. (The Σ_g eigenphase sum varies almost linearly with R and is not shown.) Especially noteworthy is the striking influence of the resonance for internuclear separations $R \geqslant 2.0\ a_0$, which extends to energies well below the peak of the enhancement at about 3 eV in the integral cross sections†.

† The values of the internuclear separation used in this study were chosen to span the dominant space of the vibrational states that participate in the transitions of interest. These values are $R = 0.5$, 0.8, 1.0, 1.2, 1.4, 1.6, 1.8, 2.0, 2.2, 2.4, and 2.5 a_0.

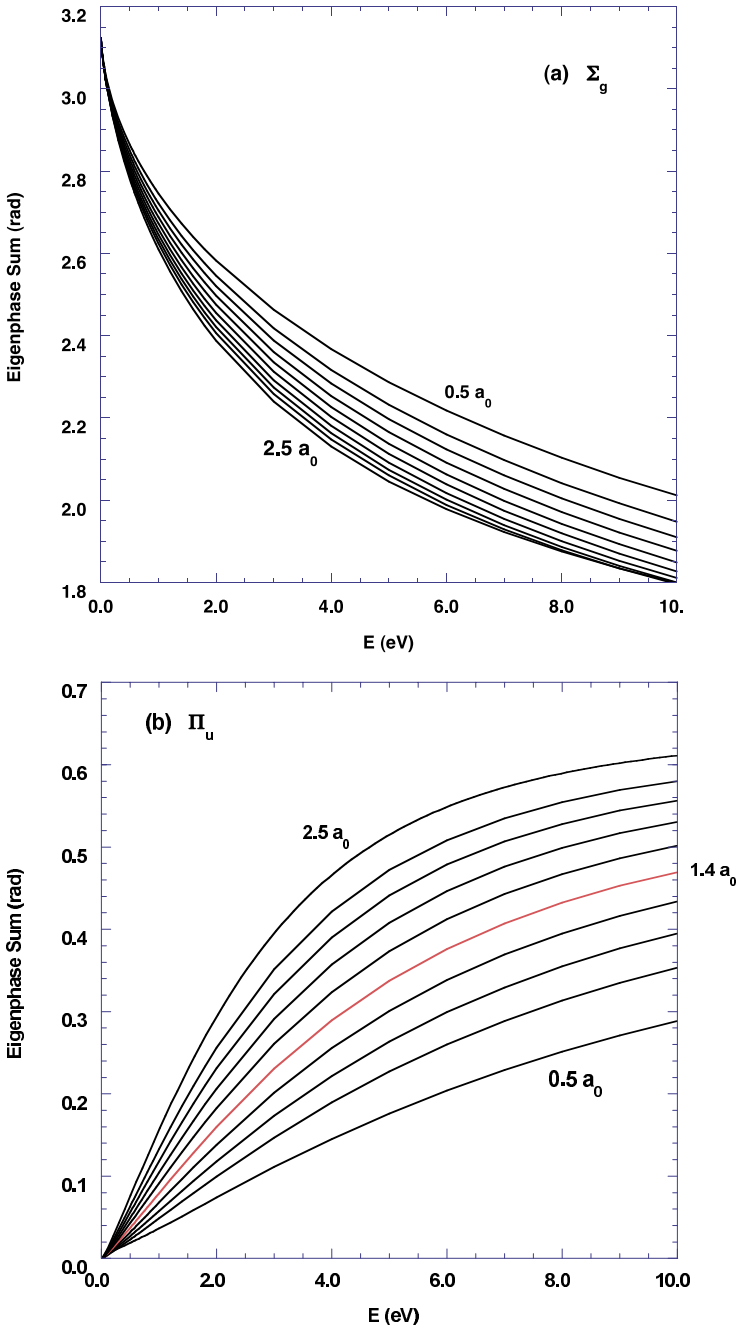

Figure 1. Fixed-nuclei eigenphase sums in the (*a*) Σ_g and (*b*) Π_u symmetries for e–H_2 scattering at selected internuclear separations R. Curves may be associated with internuclear separations by noting that the smallest eigenphase sums correspond to $R = 0.5\ a_0$. The values increase with internuclear separation for $R = 0.8$, 1.0, 1.2, 1.4, 1.6, 1.8, 2.0, 2.2, and 2.5 a_0.

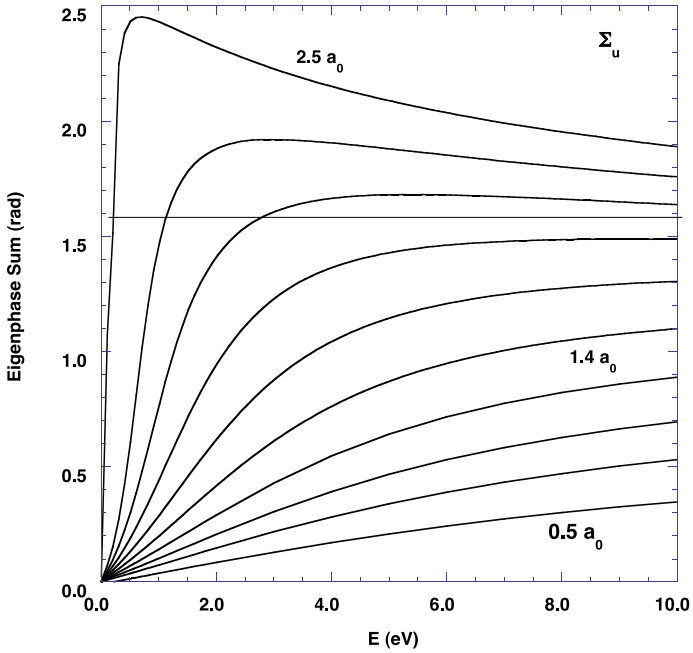

Figure 2. Fixed-nuclei eigenphase sums in the Σ_u symmetry for e–H_2 scattering for internuclear separations relevant to excitation of the $v = 1$ and $v = 2$ states. Values of R range from $R = 0.5\,a_0$ to $R = 2.5\,a_0$ and may be associated with curves as discussed in the caption to figure 1. The horizontal line corresponds to $\pi/2$ (see text).

3.4. The first-order non-degenerate adiabatic method

The key step in the FONDA method is calculation of a fixed-nuclei off-shell K-matrix $\mathcal{K}$, where we use script letters to signify off-shell scattering quantities. Conservation of energy and correct threshold-law behaviour are ensured by evaluating this matrix at a point in the complex energy plane that is appropriate to the vibrational transition of interest. Calculation of the off-shell fixed-nuclei K-matrix proceeds from the adiabatic continuum electronic wavefunction introduced in equation (6). Within this approach, the body energy is unambiguously specified so that this function is the solution of equation (4) for body energy $\epsilon = E_0$. It appears in the FONDA K-matrix elements as

$$\mathcal{K}_{\ell,\ell_0}(E_0, E_v; R) = \frac{2}{\sqrt{k_v k_0}} \sum_{\ell'} \int_0^\infty \hat{\jmath}_\ell(k_v r) V^{\Lambda}_{\ell',\ell}(r; R) w_{\ell',\ell}(r; R)\,\mathrm{d}r, \qquad (16)$$

where $V^{\Lambda}_{\ell',\ell}(r; R)$ is the fixed-nuclei potential coupling matrix element. As the internuclear separation varies, this K-matrix manifests a series of asymptotes which problematize the quadrature over R required to produce a vibronic K-matrix. Hence we first transform this fixed-nuclei off-shell K-matrix to a fixed-nuclei off-shell T-matrix with elements $\mathcal{T}_{\ell,\ell_0}(E_0, E_v; R)$. From this quantity, we evaluate the FONDA vibronic T-matrix for the transition $v_0 \rightarrow v$ by inserting $\mathcal{T}$ into an integral over R analogous to equation (3). Finally, we transform this vibronic T-matrix into the desired vibronic K-matrix. All elements of the resulting matrix obey the correct threshold laws as $k_v \rightarrow 0$, a consideration that is important for molecules with strong inter-channel coupling.

One weakness of this method as previously formulated is that the FONDA vibronic K-matrix does not satisfy strict unitarity requirements. In the present implementation, we impose

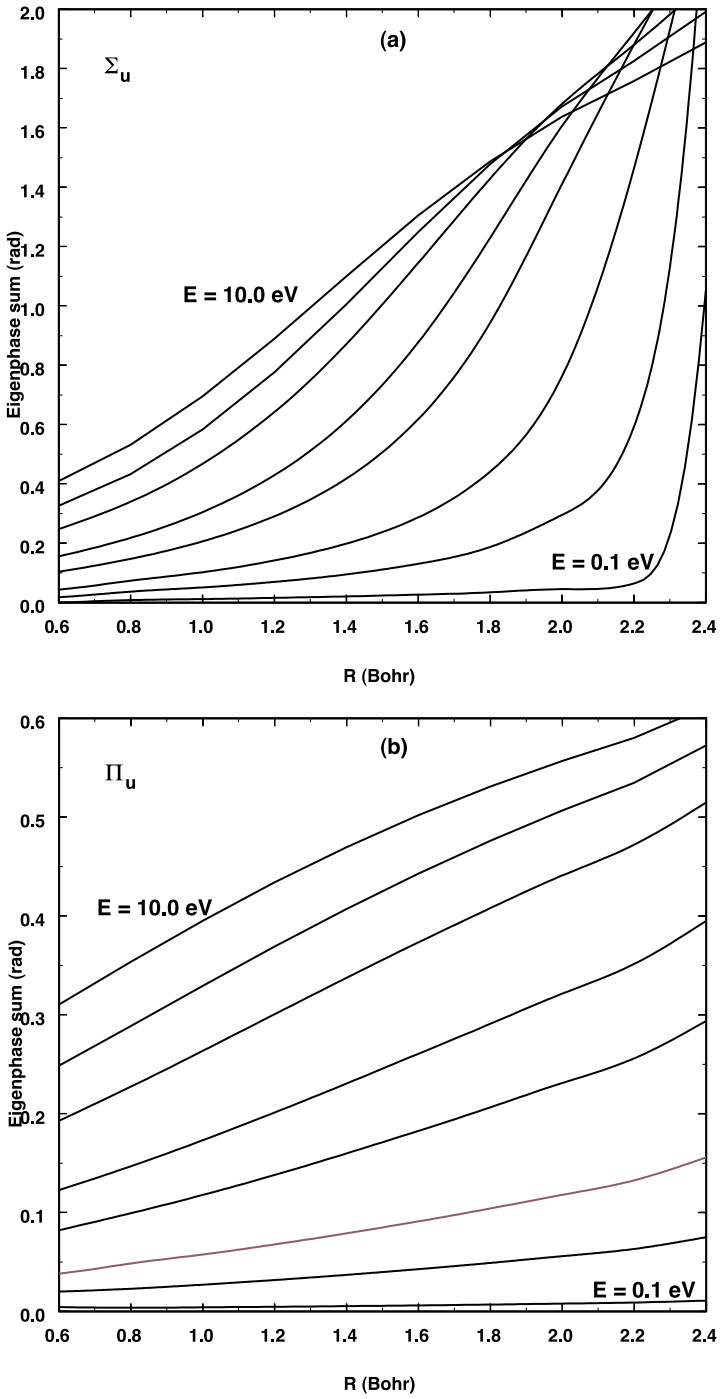

Figure 3. Fixed-nuclei eigenphase sums in the (*a*) Σ_u and (*b*) Π_u symmetries for e–H_2 scattering at selected body energies. The curves in both figures may be associated with energies by noting that at $R = 1.4\ a_0$, the smallest eigenphase sum corresponds to $\epsilon = 0.1$ eV, the next largest to 0.5 eV, and so on for the remaining energies: 1.0, 2.0, 3.0, 5.0, 7.0, and 10.0 eV.

(approximate) unitarity by ensuring that the vibronic K-matrix used to generate the relevant T-matrix elements in equation (11) is symmetric. To this end we construct this matrix as

$$\mathsf{K} = \begin{pmatrix} \mathsf{K}_{v_0 v_0} & \frac{1}{2}(\mathsf{K}_{v,v_0} + \mathsf{K}_{v_0,v}) \\ \frac{1}{2}(\mathsf{K}_{v_0,v} + \mathsf{K}_{v,v_0}) & \mathsf{K}_{vv} \end{pmatrix}. \tag{17}$$

From this we construct the final vibronic T-matrix and extract the block that corresponds to the desired transition.

3.5. Body-frame vibrational close coupling

As benchmarks for assessing the ANV, EMA, and FONDA methods we use the results of converged solutions of the Schrödinger equation for the electron–molecule wavefunction $\Psi_{E,v_0}(\boldsymbol{r}, R)$. Expansion of this function in the vibronic basis $\{\chi_v(R)Y_{\ell\Lambda}(\hat{r})\}$ leads to the coupled integrodifferential equations of the VCC method,

$$\left[\frac{\mathrm{d}^2}{\mathrm{d}r^2} - \frac{\ell(\ell+1)}{r^2} + k_v^2\right] u_{v\ell,v_0\ell_0}(r) = 2\sum_{v',\ell'}[V^{\Lambda}_{v'\ell',v\ell}(r;R) + \hat{\mathcal{V}}^{\Lambda}_{v'\ell',v\ell}(r;R)]u_{v'\ell',v_0\ell_0}(r). \tag{18}$$

The local coupling matrix elements $V^{\Lambda}_{v'\ell',v\ell}(r;R)$ contain contributions from the electrostatic (Coulomb) interaction and polarization-correlation effects; the non-local matrix elements $\hat{\mathcal{V}}^{\Lambda}_{v'\ell',v\ell}(r;R)$ allow for exchange of the continuum and bound electrons. All three contributions are based on a near-Hartree–Fock wavefunction for the ground electronic state of the target which we have described in detail elsewhere (Morrison *et al* 1984a, Gibson and Morrison 1984). We compute the local matrix elements from Legendre projections $v_\lambda(r;R)$ of the static-polarization potential as (Morrison 1980, Schmid *et al* 1980)

$$V^{\Lambda}_{v'\ell',v\ell}(r;R) = \sum_{\lambda=0}^{\infty} g_\lambda(\ell,\ell';\Lambda)\langle\chi_v|v_\lambda(r;R)|\chi_{v'}\rangle, \tag{19a}$$

where the sum over λ includes only even terms for a homonuclear target. The angular momentum coupling coefficient in equation (19*a*) is

$$g_\lambda(\ell,\ell';\Lambda) = \left(\frac{2\ell'+1}{2\ell+1}\right)^{1/2} C(\ell'\Lambda\ell;\Lambda 0\Lambda)C(\ell'\Lambda\ell;000), \tag{19b}$$

with the Clebsch–Gordan coefficients written in the notation of Rose (1957). Also appearing in the VCC equations (18) are non-local exchange matrix elements of the form

$$\hat{\mathcal{V}}^{\Lambda}_{v'\ell',v\ell}(r;R) = \int_0^{\infty} \hat{\mathcal{K}}^{\Lambda}_{v'\ell',v\ell}(r,r')u_{v\ell,v_0\ell_0}(r')\,\mathrm{d}r', \tag{19c}$$

where the kernel matrix elements $\hat{\mathcal{K}}^{\Lambda}_{v'\ell',v\ell}(r,r')$ are calculated from the bound $1\sigma_g$ molecular orbital of H_2 as detailed in Morrison (1988), Trail (1991), and Morrison and Trail (1993). Details concerning the correlation-polarization used in this study appear in Morrison and Trail (1993) and Mazevet *et al* (1999) and references therein. In the present calculations we include four vibrational states and three partial waves in the expansion of the BF scattering function for each electron–molecule symmetry. In calculating the exchange kernel in equation (19*c*), we include three partial waves in expansion of the bound molecular orbital. We propagate the radial solution matrices to 100 a_0, at which point we extract K-matrix elements. Specifically, we recast equations (18) using the linear-algebraic algorithm (Schneider and Collins 1981).

Table 2. Partial integral cross sections (in a_0^2) and their sum (the total elastic cross section) for e–H_2 scattering at selected energies from the following theories: VCC (top line for each energy), unitarized body-frame FONDA method (second line), and EMAP approximation (third line).

E	Σ_g	Σ_u	Π_u	Total
0.60	0.0126	0.0211	0.0013	0.0349
	0.0150	0.0215	0.0011	0.0376
	0.0081	0.0149	0.0008	0.0238
0.80	0.0222	0.1331	0.0063	0.1616
	0.0246	0.1369	0.0056	0.1671
	0.0187	0.1124	0.0045	0.1356
1.00	0.0284	0.3102	0.0122	0.3508
	0.0304	0.3104	0.1076	0.3516
	0.0261	0.2810	0.0090	0.3161
2.00	0.0425	1.5974	0.0382	1.6781
	0.0441	1.3900	0.0339	1.4680
	0.0438	1.5420	0.0314	1.6170
3.00	0.0471	1.8415	0.0502	1.9388
	0.0486	1.7340	0.0449	1.8270
	0.0495	1.8520	0.0429	1.9440
4.00	0.0486	1.5967	0.0505	1.6957
	0.0498	1.5310	0.0453	1.6260
	0.0514	1.5950	0.0439	1.6900
5.00	0.0488	1.2505	0.0449	1.3442
	0.0496	1.2190	0.0403	1.3090
	0.0518	1.2550	0.0393	1.3460
7.00	0.0477	0.7464	0.0301	0.8242
	0.0483	0.7387	0.0269	0.8139
	0.0506	0.7541	0.0266	0.8313
8.00	0.0469	0.5885	0.0238	0.6592
	0.0474	0.5837	0.0213	0.6524
	0.0497	0.5946	0.0211	0.6654

4. Results

4.1. The $v_0 = 0 \rightarrow v = 1$ transition

The threshold for the $0 \rightarrow 1$ excitation is at 0.5156 eV. Figure 4 shows partial integral cross sections for this excitation in the three dominant symmetries, Σ_g, Σ_u, and Π_u, and their sum, the total inelastic cross section summed over all rotational transitions. (These and other data are presented at selected energies in table 2; a full list is available on request from the authors.) These figures include results from the three adiabatic theories discussed in section 2: the ANV with the 'flux factor' correction (ANVf), the EMAP method, and the unitarized FONDA method. As benchmarks for assessing these approximate cross sections we use VCC cross sections.

Like the e–H_2 elastic cross section, the $0 \rightarrow 1$ cross section is dominated at energies below 10 eV by the Σ_u partial cross section except very near the threshold at 0.52 eV, where Σ_g takes over. Nevertheless, the Σ_g partial cross section is of considerable interest because only in this symmetry does the lowest-order partial wave ($\ell = 0$) not produce a centrifugal barrier. Hence the corresponding elements of the radial scattering function experience the full short-range interaction potential, so the cross section in this symmetry, $\sigma_{v_0 \rightarrow v}^{\Sigma_g}$, is highly sensitive to nonadiabatic and energetic effects near threshold. As figure 4(a) shows, however, all three adiabatic theories accurately reproduce this cross section, with only the EMAP results

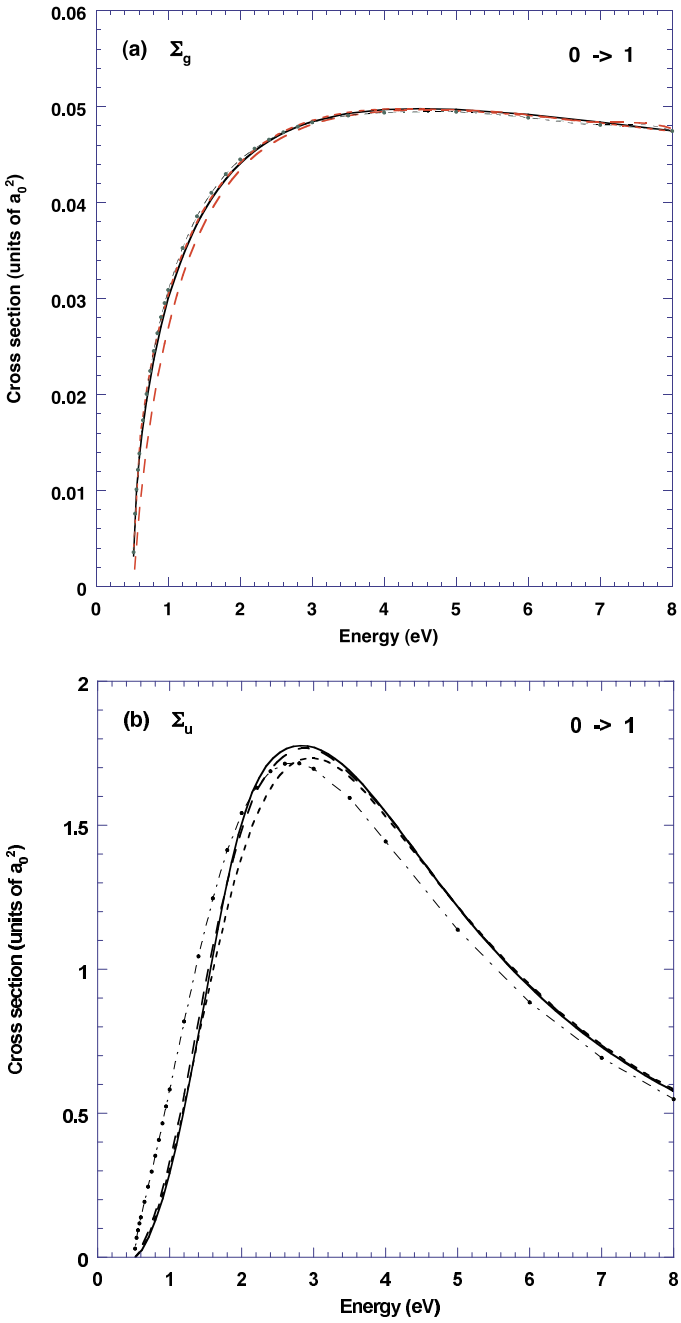

Figure 4. Partial integral cross sections in the (*a*) Σ_g, (*b*) Σ_u, and (*c*) Π_u symmetries for the $0 \rightarrow 1$ vibrational excitation of H_2 and (*d*) their sum. Results for the EMAP (long-broken curve), unitarized FONDA (short-broken curve), and ANVf (chain curve) are compared with benchmark VCC cross sections (full curve). In (*a*) and (*c*), the FONDA results are barely distinguishable from the VCC cross sections.

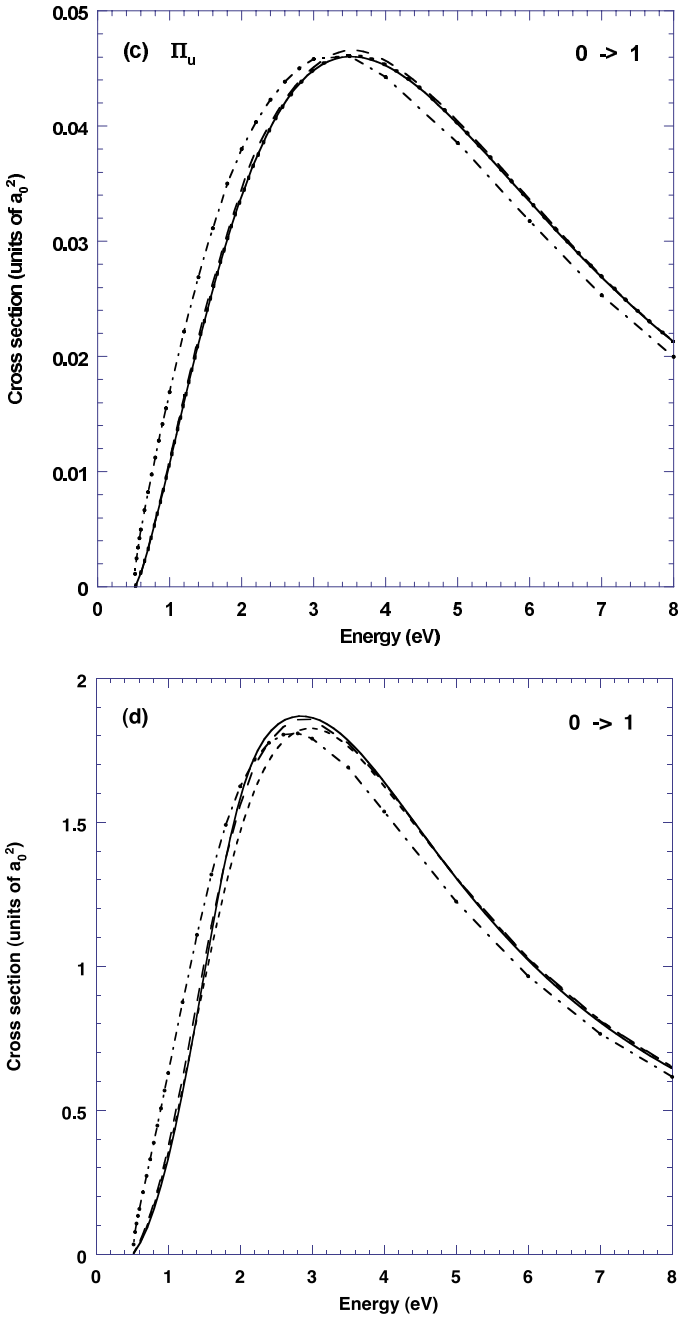

Figure 4. (Continued)

deviating from the VCC benchmarks as the energy decreases below about 3.0 eV.

In the dominant Σ_u symmetry, the threshold law (5) prescribes that $\sigma^{\Sigma_u}_{v_0\to v}$ must approach zero near threshold as k_v^3. In the EMAP method the (dominant) $\ell = 1$, $\ell_0 = 1$ matrix element goes to zero as $k_v^{3/2}$, because it is evaluated at the geometric mean. As figure 4(*b*) shows, this method yields results that agree well with the VCC cross sections. Excellent agreement is also seen in the FONDA results, as this method enforces proper threshold behaviour in all element of the T-matrix. The ANVf cross section, which goes to zero as k_v, not only suffers error at energies below the peak near 3 eV but, because it positions the peak incorrectly, is also considerably in error at energies up to several eV.

Similar behaviour for all three adiabatic theories is evident in the Π_u cross section in figure 4(*c*). This partial cross section qualitatively resembles that of the Σ_u symmetry but is much less important, being of the same order of magnitude as the $\sigma^{\Sigma_g}_{0\to 1}$. Consequently the total $0 \to 1$ integral cross section in figure 4(*d*) reflects the behaviour of the Σ_u partial cross section, both in its energy dependence and in the accuracy of the ANVf, EMAP, and FONDA approximations.

Because differential cross sections (DCS) are more sensitive than integral cross sections to errors in the T-matrix, their study can shed additional light on the merits of these approximations. Figure 5 shows $0 \to 1$ DCS from EMAP and FONDA calculations at four energies chosen to illustrate trends in their accuracy as energy increases from threshold. (Studies of DCS in the ANV and ANVf approximations appear in Morrison *et al* (1984b, 1991).) At the lowest energy shown, 0.8 eV in figure 5(*a*), the threshold laws for key T-matrix elements in the contributing symmetries play a sufficiently important role in the DCS that the FONDA result more closely approximates the VCC cross sections than does the EMAP, especially at small and intermediate angles.

By twice this energy, 1.6 eV in figure 5(*b*), the importance of the threshold behaviour is significantly diminished, and both adiabatic methods give good agreement with the VCC benchmarks. This tendency continues with further increases in energy. The 2.0 eV comparison in figure 5(*c*) appears to favour the FONDA cross section, but as the 3.0 eV results in figure 5(*d*) show, this agreement is fortuitous, a consequence of the EMAP cross section changing from slightly below than the VCC result (figure 5(*b*)) to slightly above (figure 5(*d*)). With still further increases in energy (not shown), both approximate DCS become indistinguishable from their VCC counterparts, within the roughly 1% accuracy of these calculations.

4.2. The $v_0 = 0 \to v = 2$ transition

Our results for the $0 \to 1$ integral and differential cross sections demonstrate the ability of both the EMAP and FONDA methods to approximate accurately the scattering dynamics from threshold to 10 eV for this excitation. Operationally, however, the EMAP method is easier to implement and less demanding computationally than the FONDA approximation. To explore further the viability of this method, we now turn to the $0 \to 2$ excitation. In e–H_2 scattering, higher excitations tax any adiabatic method, since nonadiabatic effects become more important in the vicinity of the resonance at about 3.0 eV (Allen 1985). Even though the motion of the resonance pole of the S-matrix away from the real axis with decreasing internuclear separation makes the influence of this pole on $0 \to 1$ scattering is negligible, this is not true for higher excitations. Here the larger expanse of the final-state vibrational wavefunction places more emphasis on large values of R, making the fixed-nuclei resonance pole and the attendant nonadiabatic effects more important.

This feature of $0 \to 2$ scattering is evident in figures 6(*a*)–(*d*), which show integral cross sections from EMAP, ANVf, and VCC calculations. The most significant differences between

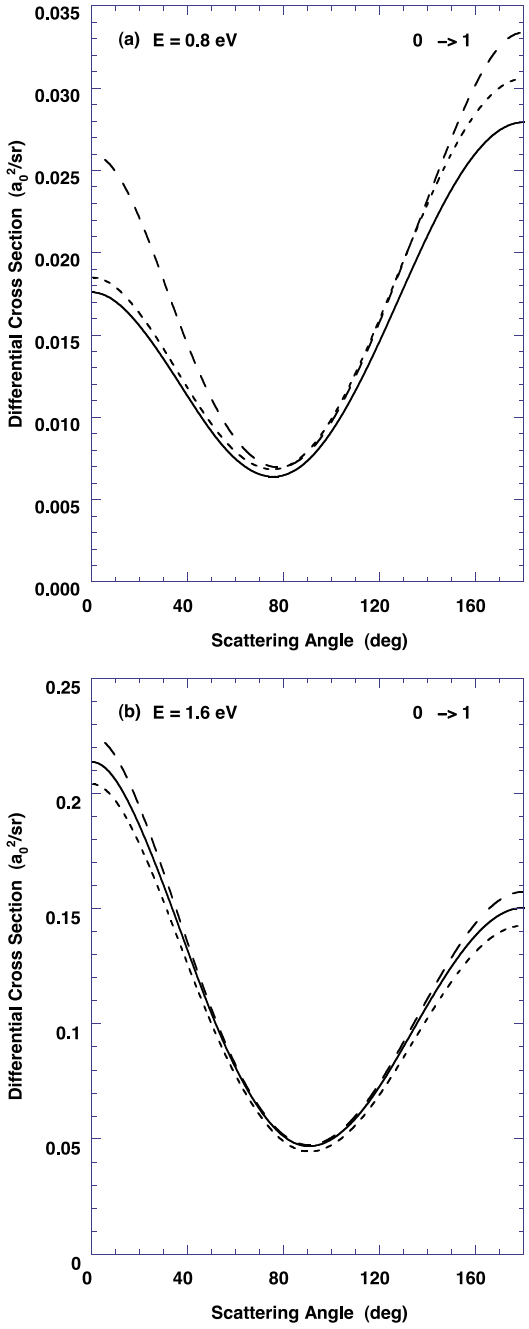

Figure 5. Differential cross sections for the $0 \rightarrow 1$ vibrational excitation of H_2 at (*a*) 0.8, (*b*) 1.6, (*c*) 2.0, and (*d*) 3.0 eV. Results for the EMAP (long-broken curve) and unitarized FONDA (short-broken curve) approximations are compared with benchmark VCC results (full curve).

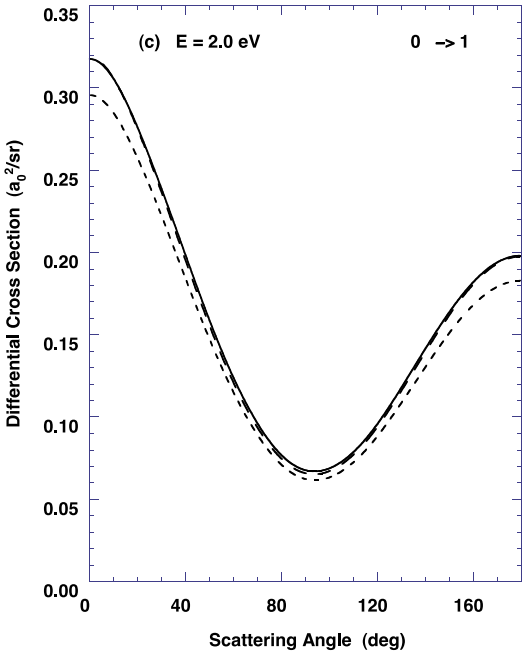

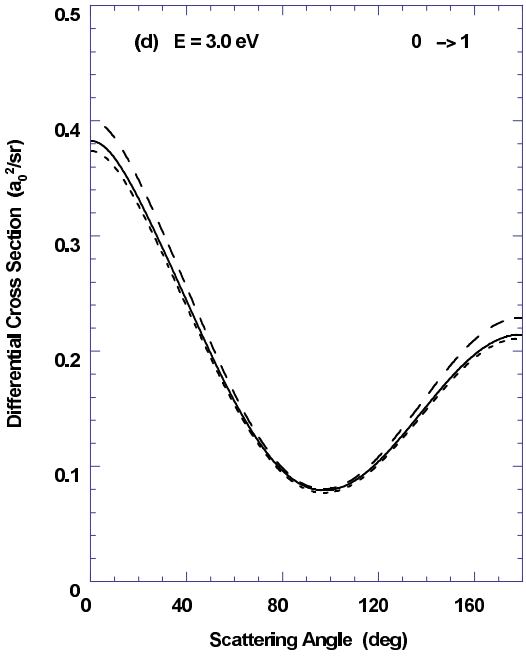

Figure 5. (Continued)

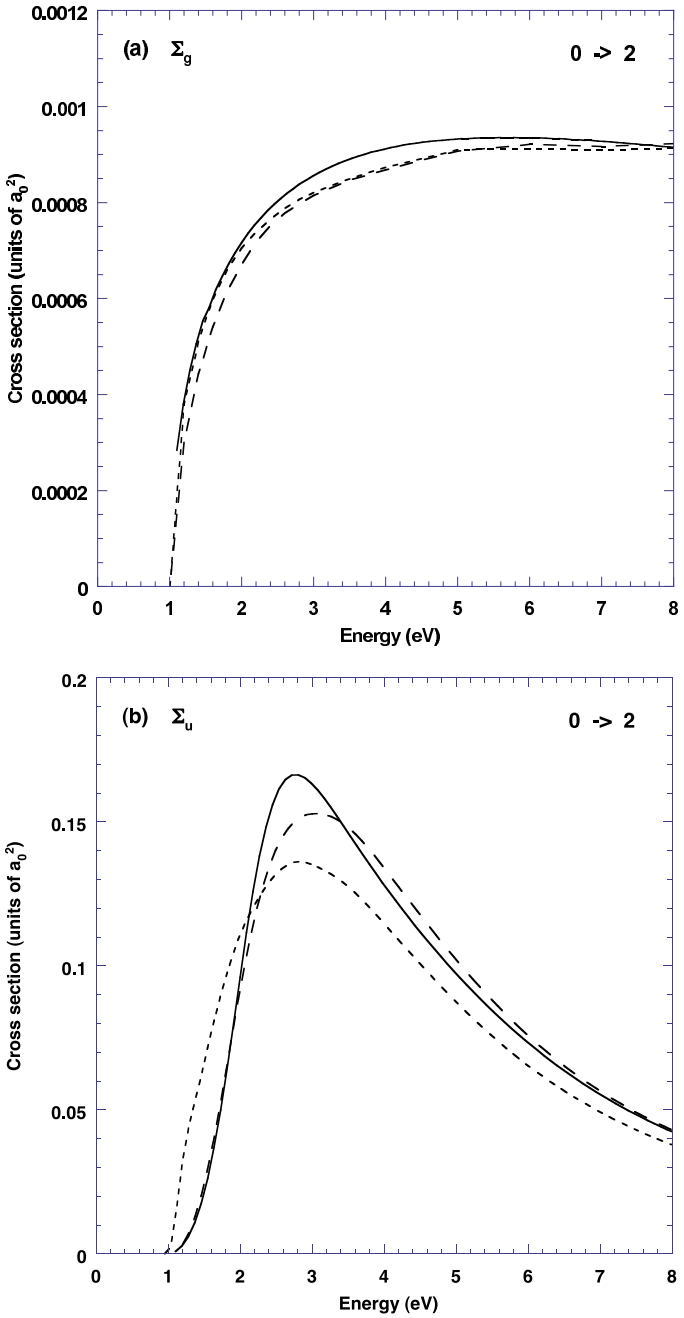

Figure 6. Partial integral cross sections in the (*a*) Σ_g, (*b*) Σ_u, and (*c*) Π_u symmetries for the $0 \rightarrow 2$ vibrational excitation of H_2 and (*d*) their sum. Results for the EMAP (long-broken curve) and ANVf (short-broken curve) are compared with benchmark VCC cross sections (full curve).

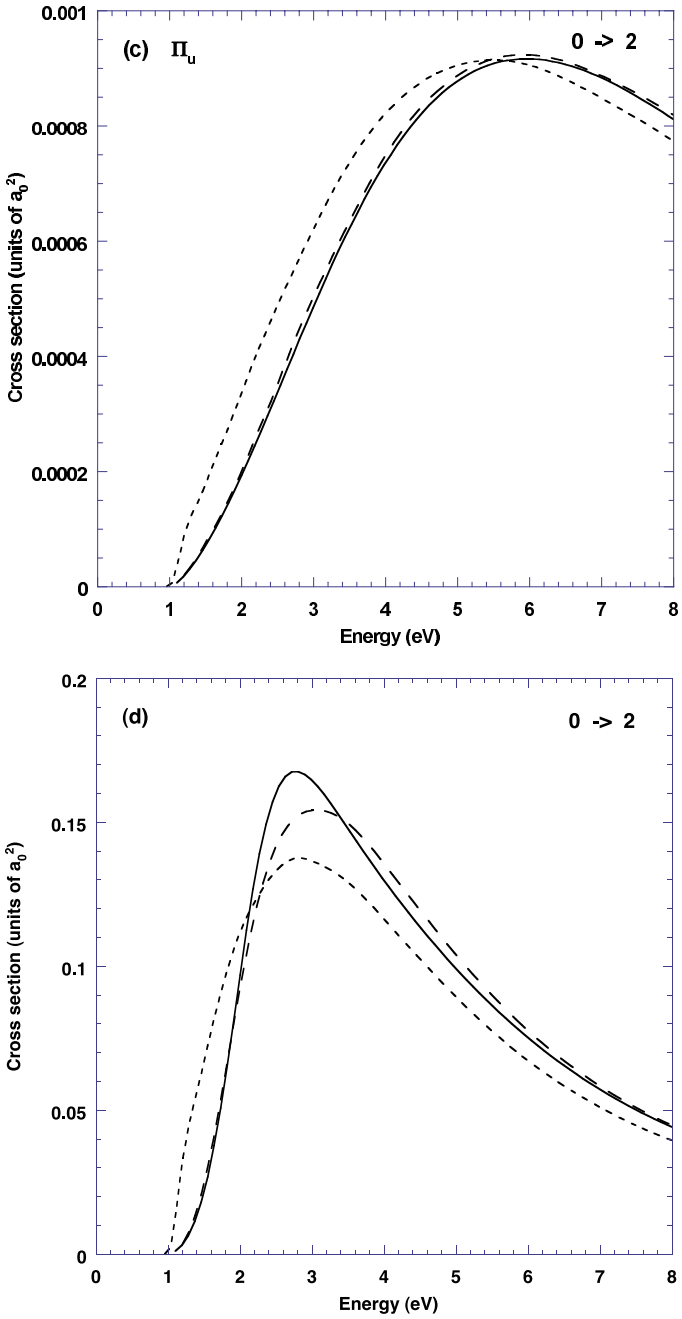

Figure 6. (Continued)

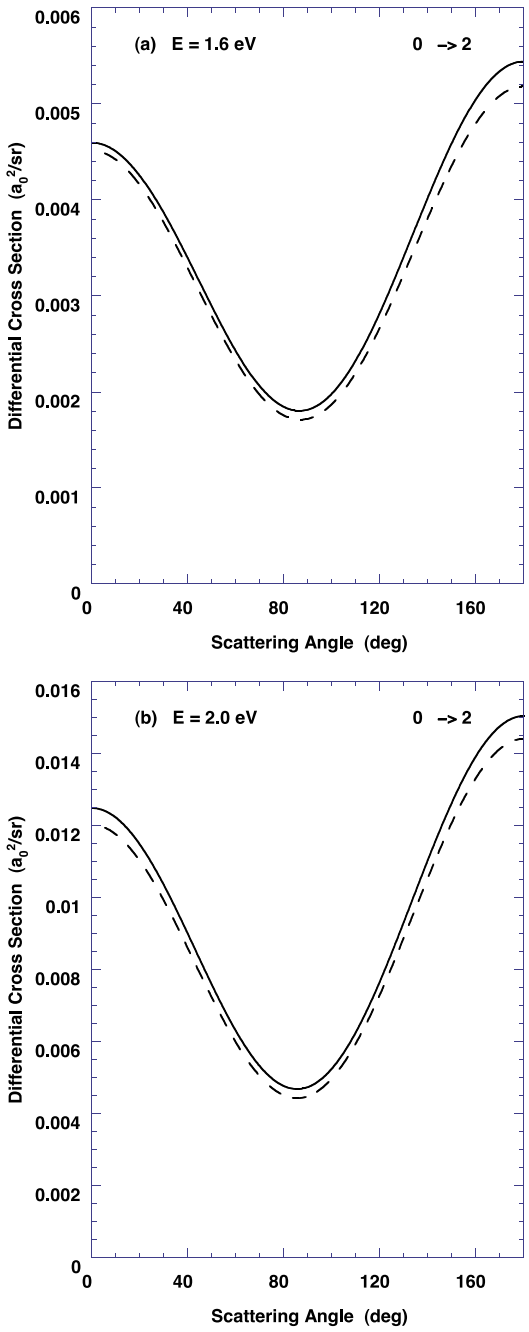

Figure 7. Differential cross sections for the $0 \rightarrow 2$ vibrational excitation of H_2 at (*a*) 1.6, (*b*) 2.0, (*c*) 3.0, and (*d*) 3.5 eV. Results for the EMAP (long-broken curve) approximation are compared with benchmark VCC results (full curve).

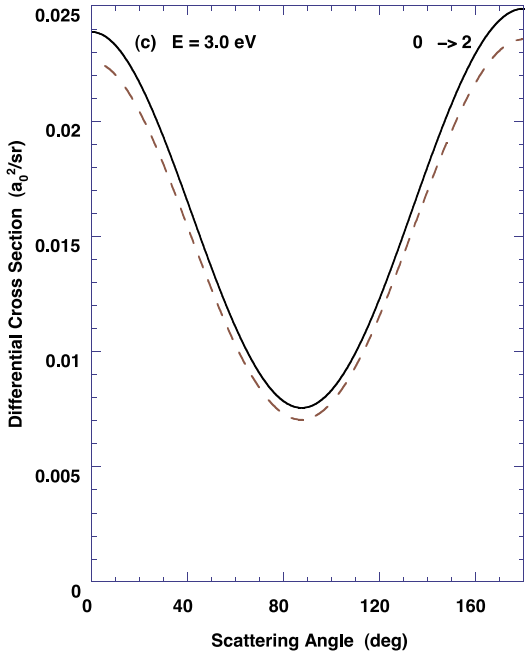

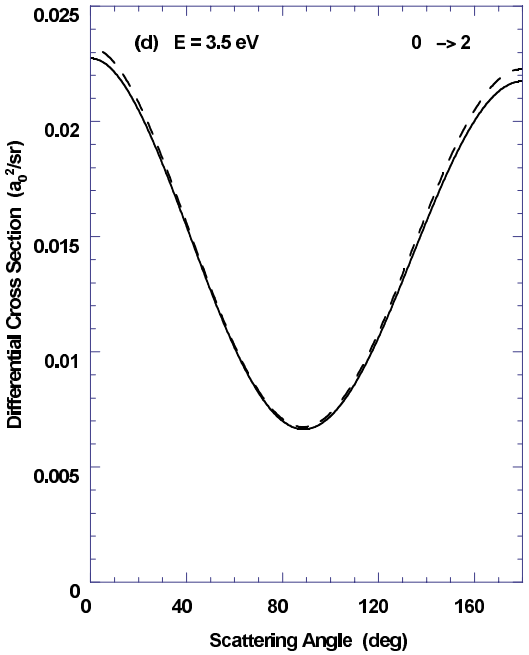

Figure 7. (Continued)

the adiabatic (EMAP and ANVf) and nonadiabatic (VCC) results are in the resonant Σ_u cross sections in figure 6(*b*). Here the EMAP method reproduces the correct near-threshold cross section but not the resonance peak. In the vicinity of this peak, from about 2.0 eV to about 5.0 eV, one must include nonadiabatic effects, as is done through vibrational coupling in the VCC calculations or through construction of a vibronic R-matrix in the nonadiabatic phase matrix method (Nesbet 1996, Mazevet *et al* 1999). These substantive errors in the adiabatic Σ_u cross sections for this excitation infect, of course, the total $0 \rightarrow 2$ cross section in figure 6(*d*).

Differential cross sections for this excitation are shown in figure 7. The first of these figures, figure 7(*a*), shows that the EMAP method yields a very good approximation to the VCC cross section even at a scattering energy (1.6 eV) that is near the threshold at 1.001 127 eV. As the energy increases through the resonance to 3.5 eV in figures 7(*b*)–(*d*), this agreement deteriorates slightly due to the increased importance of nonadiabatic effects. Still, even here the shape of the EMAP cross section is very close to that of its VCC counterpart. At still higher energies (not shown), the EMAP and VCC results merge, as they should.

5. Conclusions

The results of this study argue strongly for the EMAP method as a computationally efficient way to generate reasonably accurate integral and differential cross sections at energies somewhat above threshold, except far from a resonance whose character reflects conditions where nonadiabatic effects are important. In support of this assertion, the present study of e–H_2 scattering complements previous work by Thümmel *et al* (1993) on e–HF collisions. For near-threshold scattering, where correct adherence by key T-matrix elements to the threshold law (5) is important and conservation of energy during the collision (1) must be maintained, either converged VCC calculations or a method such as the FONDA approximation should be used if accurate cross sections are required. For energies near most shape resonances, one must use a method that explicitly incorporates nonadiabatic physics, such as VCC, nonadiabatic R-matrix theory, projection operator approaches, or the nonadiabatic phase matrix method (Mazevet *et al* 1999). While the exceptionally broad and ill-defined 'resonance' in the $0 \rightarrow 1$ e–H_2 cross section is a notable exception to this rule, it is important to note that even for this system, nonadiabatic effects become much more important with increasing final-state vibrational quantum number, as illustrated by figures 4 and 6.

In all other circumstances, the EMAP method, applied directly to the K-matrix using the geometric mean for off-diagonal elements as in section 2, provides cross sections whose accuracy is comparable with that of VCC or FONDA results with a lot less work. For most electron–molecule systems, converging VCC calculations is impractical even on today's supercomputers; in fact no converged VCC calculations which include the vibrational continuum have been reported. The FONDA approximation avoids vibrational coupling altogether but at the cost of explicitly evaluating off-shell T-matrix elements—a chore that can be rather computationally demanding, especially for excitations with $\Delta v > 1$. By working entirely with on-shell fixed-nuclei K-matrices, the EMAP method facilitates implementation with little more work than a conventional adiabatic-nuclei (ANVf) calculation. Yet because of its improved treatment of the dependence on the exit-channel energy of (low-energy) K-matrix elements, this method can yield significantly more accurate results, especially for differential cross sections, even at energies as high as 10 eV. These conclusions are supported by the comparisons of EMAP $0 \rightarrow 1$ and $0 \rightarrow 2$ integral and differential cross sections in section 4.

Acknowledgments

We would like to thank Dr Wayne K Trail for his assistance with the VCC calculations reported here, Dr Barry I Schneider for useful discussions, and the National Science Foundation for support under grant no PHY-9722055.

References

Abdolsalami M and Morrison M A 1987 *Phys. Rev.* A **36** 5474–7
Allan M 1985 *J. Phys. B: At. Mol. Phys.* **18** L451–5
Chandra N and Temkin A 1976 *Phys. Rev.* A **13** 188–203
Chang E S and Fano U 1982 *Phys. Rev.* A **6** 173–85
Chang E S and Temkin A 1970 *J. Phys. Soc. Japan* **29** 172–9
Chase D M 1956 *Phys. Rev.* **104** 838–42
Collins L A and Schneider B I 1981 *Phys. Rev.* A **24** 2387–401
Crompton R W and Morrison M A 1993 *Aust. J. Phys.* **46** 203–30
DeRose E, Gislason E A and Sabelli N H 1985 *J. Chem. Phys.* **82** 4577–84
Domcke W 1991 *Phys. Rep.* **208** 97–188
Faisal F H M and Temkin A 1972 *Phys. Rev. Lett.* **28** 203–6
Gibson T L and Morrison M A 1984 *Phys. Rev.* A **29** 2479–508
Gorczyca T and Norcross D W 1990 *Phys. Rev.* A **42** 5132–8
Hara S 1969 *J. Phys. Soc. Japan* **27** 1592–7
Hazi A 1979 *Phys. Rev.* A **19** 920–2
Henry R J W 1970 *Phys. Rev.* A **2** 1349–58
Isaacs W A and Morrison M A 1998 *Phys. Rev.* A **57** R9–12
Lane N F 1980 *Rev. Mod. Phys.* **52** 29–119
Mazevet S, Morrison M A, Boydstun O and Nesbet R K 1999 *Phys. Rev.* A **59** 477–89
Mazevet S, Morrison M A, and Nesbet R K 1998 *J. Phys. B: At. Mol. Opt. Phys.* **31** 4437–48
McCurdy C W and Mowrey R C 1982 *Phys. Rev.* A **25** 2529–38
Meyer H D, Pal S and Riss U B 1992 *Phys. Rev.* A **46** 186–93
Morrison M A 1980 *Comput. Phys. Commun.* **21** 63–77
——1986 *J. Phys. B* **19** L707–715
——1988 *Adv. At. Mol. Phys.* **24** 51–156
Morrison M A, Abdolsalami M and Elza B K 1991 *Phys. Rev.* A **43** 3440–59
Morrison M A, Crompton R W, Saha B C and Petrovič Z L 1987 *Aust. J. Phys.* 40
Morrison M A, Feldt A N and Austin D 1984a *Phys. Rev.* A **29** 2518–40
Morrison M A, Feldt A N and Saha B C 1984b *Phys. Rev.* A **30** 2811–13
Morrison M A and Sun W 1995 *Computational Methods for Electron–Molecule Collisions* ed W Huo and F Gianturco (New York: Plenum) ch 6, pp 131–90
Morrison M A and Trail W K 1993 *Phys. Rev.* A **48** 1874–2886
Nesbet R K 1979 *Phys. Rev.* A **19** 551–6
——1991 *Collision Processes of Ion, Positron, Electron and Photon Beams with Matter (Latin American School of Physics)* ed A C de Azevedo e Souza *et al* (NJ: World Scientific) pp 94–103
——1996 *Phys. Rev.* A **54** 2899
Nesbet R K, Noble C J, Morgan L A and Weatherford C A 1984 *J. Phys. B: At. Mol. Phys.* **17** L891–5
Rose M E 1957 *Elementary Theory of Angular Momentum* (New York: Wiley)
Schmid G B, Norcross D W and Collins L A 1980 *Comput. Phys. Commun.* **21** 79–90
Schneider B I and Collins L A 1981 *Phys. Rev.* A **24** 1264–6
Schneider B I, Dourneuf M L and Burke P G 1979 *J. Phys. B: At. Mol. Phys.* **12** L365–9
Shugard M and Hazi A U 1975 *Phys. Rev.* A **12** 1895–902
Sun W, Morrison M A, Isaacs W A, Trail W K, Alle D T, Gulley R J, Brennan M J and Buckman S J 1995 *Phys. Rev.* A **52** 1229–56
Taylor J R 1972 *Scattering Theory* (New York: Wiley)
Temkin A and Vasavada K V 1967 *Phys. Rev.* **160** 109–17
Thümmel H T, Grimm-Bosbach T, Nesbet R K and Peyerimhoff S D 1995 *Computational Methods for Electron–Molecule Collisions* ed W M Huo and F A Gianturco (New York: Plenum) ch 12, pp 265–92
Thümmel H T, Nesbet R K and Peyerimhoff S D 1992 *J. Phys. B: At. Mol. Opt. Phys.* **25** 4533–79

——1993 *J. Phys. B: At. Mol. Opt. Phys.* **26** 1233–51
Trail W K 1991 Exchange in vibrational excitation of small molecules by electron impact *PhD Thesis* University of Oklahoma
Trail W K, Morrison M A, Isaacs W A and Saha B C 1990 *Phys. Rev.* A **41** 4868–78
Weatherford C A and Temkin A 1994 *Phys. Rev.* A **49** 2580–6